Determination of the Metallic/Semiconducting Ratio in Bulk Single-Wall Carbon Nanotube Samples by Cobalt Porphyrin Probe Electron Paramagnetic Resonance Spectroscopy

Sofie Cambré,[†,*] Wim Wenseleers,[†] Etienne Goovaerts,[†] and Daniel E. Resasco[‡]

[†]Department of Physics, University of Antwerp, Universiteitsplein 1, 2610 Antwerp, Belgium, and [‡]School of Chemical, Biological and Materials Engineering, University of Oklahoma, 100 East Boyd Street, Norman, Oklahoma 73019, United States

ABSTRACT A simple and quantitative, self-calibrating spectroscopic technique for the determination of the ratio of metallic to semiconducting single-wall carbon nanotubes (SWCNTs) in a bulk sample is presented. The technique is based on the measurement of the electron paramagnetic resonance (EPR) spectrum of the SWCNT sample to which cobalt(II)octaethylporphyrin (CoOEP) probe molecules have been added. This yields signals from both CoOEP molecules on metallic and on semiconducting tubes, which are easily distinguished and accurately characterized in this work. By applying this technique to a variety of SWCNT samples produced by different synthesis methods, it is shown that these signals for metallic and semiconducting tubes are independent of other factors such as tube length, defect density, and diameter, allowing the intensities of both signals for arbitrary samples to be retrieved by a straightforward least-squares regression. The technique is self-calibrating in that the EPR intensity can be directly related to the number of spins (number of CoOEP probe molecules), and as the adsorption of the CoOEP molecules is itself found to be unbiased toward metallic or semiconducting tubes, the measured intensities can be directly related to the mass percentage of metallic and semiconducting tubes in the bulk SWCNT sample. With the use of this method it was found that for some samples the metallic/semiconducting ratios strongly differed from the usual 1:2 ratio.

KEYWORDS: electronic type · spin probe EPR · CoMoCat · SWCNTs · electron spin resonance · metallic:semiconducting ratio · EPR spectroscopy

Single-wall carbon nanotubes (SWCNTs) have attracted tremendous interest because of their unique electronic, optical, thermal, and mechanical properties which are particularly promising for a wide range of applications in (nano)opto-electronics. However, a major obstacle for these applications is the fact that the electronic properties of SWCNTs depend critically on their exact chiral structure (chiral index (n,m)),[1] and all synthesis methods known to date produce a mixture of both metallic (M) and semiconducting (SC) SWCNTs. For a few years now, significant progress is being made in the preparation of SWCNT samples enriched in either semiconducting or metallic tubes, either at the synthesis level[2−6] or by various post-growth separation methods.[7−17] One of the most promising separation methods is density gradient centrifugation[7] of bile salt solubilized[18] SWCNTs, which not only allows the separation of semiconducting and metallic tubes but can also sort them according to chirality and even handedness.[19] However, characterizing the actual content of semiconducting and metallic SWCNTs in a bulk sample remains difficult, because no simple spectroscopic technique giving a reliable, absolute reading of the M:SC ratio was available until now. Here, we show that the electron paramagnetic resonance (EPR) spectrum of a bulk sample of SWCNTs, to which Co(II)octaethylporphyrin (CoOEP) probe molecules have been added, directly yields such a measurement of the M:SC ratio in the original SWCNT sample, without requiring an external calibration, yielding a simple, quantitative spectroscopic technique for the determination of M:SC ratios in bulk SWCNT samples.

Several spectroscopic techniques have been proposed in literature for characterizing the M:SC ratio of SWCNT samples. A 2D Raman map, over a sufficiently wide range of laser wavelengths to cover resonances of all SWCNT chiralities in a given sample can in principle be used to determine the complete chirality distribution and hence also the M:SC ratio.[20] However, this is extremely tedious and not feasible for arbitrary diameter ranges (limited by the available lasers and detection wavelength range). Moreover, resonant Raman scattering data are difficult to quantify because these depend

*Address correspondence to sofie.cambre@ua.ac.be.

Received for review August 31, 2010 and accepted October 12, 2010.

Published online October 19, 2010.
10.1021/nn102222w

on the accurate knowledge of the Raman cross sections for SWCNTs of different chiralities and electronic type, which are currently only available from theoretical calculations,[21−23] and the effects of surfactant coating, defects, *etc.* are not well understood. Optical absorption spectroscopy may be useful for samples including only large diameter tubes with a narrow diameter distribution, such that the first two transitions of the semiconducting tubes and the first transition of the metallic tubes all lead to well-separated absorption bands. Even then, the absorption cross section of the M and SC tubes needs to be calibrated first by measurements on fully separated samples.[24] This calibration would have to be redone for each batch of SWCNTs having a different diameter distribution. When samples contain thin tubes and/or a broader diameter distribution, the different transitions of M and SC tubes overlap, and a determination of composition can only be attempted by elaborate curve fitting,[25] which is very sensitive to the accurate knowledge of peak positions, shapes, and absorption cross sections of all individual tube chiralities. These parameters are again dependent on surfactant coating, defects, aggregation, and possibly even tube length.[26]

As a result, for the characterization of the M:SC ratio, researchers mainly had to resort to statistics made from microscopic techniques, ranging from electronic transport measurements in hundreds of single tube field-effect transistors,[3] even in combination with optical absorption spectroscopy,[27] to electric force microscopy[28] and, very recently,[29] a new counting-based method was developed using a combination of atomic force microscopy (showing both M and SC tubes) and IR fluorescence microscopy (SC only). While promising, obtaining good statistics from most of these techniques is tedious, and generally it is difficult to exclude a bias (both in sample deposition and in the actual measurements) toward different SWCNT types, lengths, bundles, *etc.*

While EPR in general has been used in the study of carbon nanotubes[30−34] or their inclusion complexes,[32,35−38] the use of spin probe EPR spectroscopy for the characterization of the properties of the SWCNTs remains largely unexplored. Porphyrin molecules are interesting candidates as they are known to interact strongly with SWCNTs[39−42] and can contain various metal ions which can be probed by EPR.[43] Very recently,[44] we used EPR spectroscopy to study the interactions between Cobalt(II)octaethylporphyrins (CoOEP) and CVD-grown SWCNTs with a diameter distribution centered around 2 nm and found that the CoOEP molecules adsorb very strongly on both M and SC tubes by π-stacking. However the M tubes act as stronger electron acceptors (for the spin density on CoOEP), leading to a significant difference between the EPR spectra of porphyrins adsorbed on M and SC tubes. As a result, the EPR spectra of the functionalized SWCNT powders consist of two well-resolved components, one associated with the molecules coating the M tubes and the other with those coating the SC tubes. This is very promising as a tool to characterize the M:SC ratio in a SWCNT sample, as EPR spectroscopy is intrinsically quantitative: the integrated EPR signals can be directly related to the number of spins (CoOEP molecules) contributing to the two signals. As the two component signals were also found to occur in a constant relative intensity, independent of the procedure used in rinsing off the excess (unbound) molecules (*i.e.*, the molecules are not preferentially removed from one or the other electronic type of SWCNTs), the intensities of both signals are proportional to the surface area and hence the mass fraction of M and SC tubes, respectively. Therefore, we set out to investigate whether Co porphyrin probe EPR spectroscopy can be elaborated as a simple and reliable technique to determine M:SC ratios of bulk samples, and we applied it to a representative series of SWCNT samples, in order to demonstrate its independence on other factors such as tube diameter and diameter distribution, tube length, and defects.

RESULTS AND DISCUSSION

Methodology. The EPR spectrum of CoOEP-functionalized SWCNTs, measured in an oxygen-poor (nitrogen) atmosphere, contains two well-resolved signals from both CoOEP molecules adsorbed on metallic (M) and on semiconducting (SC) tubes, which can be easily distinguished from each other, and which are different from that of the pure, unbound CoOEP.[44] In the presence of oxygen, a third component occurs, which could be assigned to oxygenated CoOEP molecules ($Co^{III}-O_2^-$).[44−46] It was established that the molecular oxygen binds exclusively to porphyrins adsorbed on SC SWCNTs (further abbreviated as SC/O_2) and therefore the determination of the M:SC ratio is possible even in the presence of oxygen. To a first approximation, the double integral of the (first derivative) EPR signals might be used to quantify these contributions. This is sufficiently accurate in the case of the oxygen-free spectra.[44] However, the EPR intensity of the powder spectrum is also dependent on the *g*-eigenvalues.[47,48] An exact, yet simple, approach to quantify the signals is to simulate the spectra (*e.g.*, using EasySpin[47]), which implicitly accounts for these *g*-dependent prefactors, and to fit the experimental spectra with a superposition S of three of such simulations S_i (S_1 for M, S_2 for SC, and S_3 for the SC/O_2):

$$S = a_1S_1 + a_2S_2 + a_3S_3 \qquad (1)$$

where the coefficients a_i directly yield the relative concentrations of the three components in the EPR spectrum (numbers of spins), and thus of the three CoOEP species. In our previous work,[44] it was moreover established that the relative intensities of the signals associ-

TABLE 1. EPR Simulation Parameters of the Three Spectral Components, M, SC, and SC/O_2, Obtained from the Simultaneous Fit of All the EPR Spectra

	$g_\perp$	$g_\parallel$	$A_\perp$ [MHz]	$A_\parallel$ [MHz]	$g_\perp$-strain	$A_\perp$-strain [MHz]	$A_\parallel$-strain [MHz]
M[a]	3.280 ± 0.07	1.82 ± 0.04	1135 ± 10	559 ± 20	0.14 ± 0.04	80 ± 15	237 ± 50
SC[a]	3.19 ± 0.02	1.80 ± 0.04	1080 ± 10	536 ± 20	0.20 ± 0.03	85 ± 15	170 ± 50

	g_1	g_2	g_3	A_1 [MHz]	A_2 [MHz]	A_3 [MHz]	β
SC/O_2[b]	1.93	1.98	2.05	92	85	38	39°

[a]Axial **g**- and hyperfine tensors and a Lorentzian line width of $\Delta_{iso} = 6$ mT and $g_\parallel$-strain = 0 were used. [b]Orthorhombic **g**- and hyperfine tensors were used, with the Euler angles between both frames being (0°, β, 0°) with a Lorentzian isotropic line width of $\Delta_{iso} = 4$ mT, and an anisotropic Gaussian line broadening for g_1, g_2, and g_3 of 48, 45, and 17 MHz, respectively.

ated with CoOEP on M and SC tubes are constant, independent of the rinsing procedure used to remove the excess (unbound) molecules. This implies that the adsorption of CoOEP molecules is unbiased to M or SC tubes. The coefficients a_1 and $a_2 + a_3$ (which have to be added to obtain the total SC fraction) are therefore proportional to the surface area, and hence the mass fraction, of the M and SC tubes, respectively. To allow these coefficients to be quantified for an arbitrary sample by a fit of the EPR spectrum, the three component spectra S_i need to be known accurately. To this end, we studied a wide range of SWCNT materials (see Methods section for details) with different M:SC ratios by CoOEP probe EPR, which will allow the EPR parameters of S_i to be determined with great precision by a simultaneous fit of all spectra, using common magnetic parameters (including strains) and allowing only the coefficients (amplitudes) of the three components to vary between samples. In this way also the fits of the EPR spectra from CoOEP/CVD nanohybrids in our previous work could be improved significantly (see further in Figure 2). Each component spectrum, for each set of magnetic parameters, was simulated using the EasySpin software package[47] (version 3.1.0), which was called from within MatLab, in which the fitting procedure was implemented. For optimal computational efficiency and robustness, a hybrid numerical and analytical least-squares fitting procedure was used: The magnetic parameters of the three component spectra were optimized using a numerical least-squares minimization, while their amplitudes were determined (for each set of magnetic parameters tried) using an analytical (linear) least-squares regression. Having determined this set of magnetic parameters of the three species accurately (see Table 1), the EPR spectrum for any other SWCNT sample can be modeled by a linear combination of these same three components, requiring only the analytical (thus robust) linear least-squares regression. The M:SC ratio follows directly from the three coefficients.

As the various SWCNT materials studied are produced by synthesis methods involving various transition metal catalysts, they often contain ferromagnetic metal nanoparticles which give rise to large background signals in EPR.[32−34,36] These can be reduced by chemical purification, but the residual backgrounds still need to be subtracted, and can be determined by measuring the pure SWCNT materials before addition of CoOEP (see Supporting Information). Only in the case of the HipCO materials, which contain iron particles (even in the most purified grade), the ferromagnetic background, combined with the highly compacted, aggregated structure of the purified material (limiting its dispersion in chloroform and thereby limiting the amount of CoOEP molecules adsorbed on the SWCNTs, as also confirmed by optical absorption spectroscopy after solubilization of the CoOEP/HipCO nanohybrids in D_2O using bile salt surfactants; see below) prevented a sufficient signal-to-noise ratio to be achieved.

Optical Absorption Spectroscopy. To verify the proper formation of the nanohybrids in all cases, and to further study the interaction between the SWCNTs and the CoOEP molecules, the samples were also investigated by optical absorption spectroscopy after solubilization in D_2O using the bile salt surfactant sodium deoxycholate.[18] We have shown before[44] that in this way the nanohybrids can be purified yielding solutions in which at least 99% of the porphyrins are interacting with the SWCNTs. The CoOEP absorption bands, superimposed on the SWCNT background absorption, show a sizable CoOEP adsorption on the SWCNTs (see Supporting Information, Figures S3−S8;), except in the HipCO samples (Supporting Information, Figure S9), where only a minute amount of CoOEP is present. This is in line with the weak EPR signals obtained for the latter. The poor adsorption of CoOEP on the HipCO samples is not surprising, as even visually, the purified HipCO materials consist of large, compact grains which are very hard to disperse in chloroform.

Taking a closer look at the CoOEP absorption bands, after subtraction of the SWCNT absorption and a 1/wavelength scattering background, we observe a large redshift (up to 15 nm) of the CoOEP Soret band compared to the free CoOEP absorption (Figure 1), indicating a strong electronic communication between the porphyrin π-system and the SWCNT walls, in agreement with the EPR results. Interestingly, this red shift is found to depend on the SWCNT sample used (Table 2). For CVD SWCNTs, a spectral shift of 15 nm is observed, in line with previous work.[44] The smallest shift, of 10 nm,

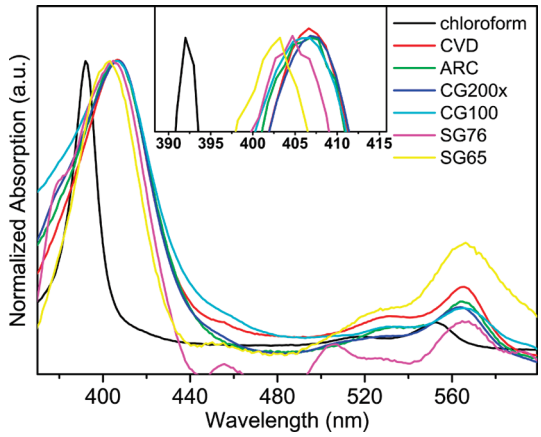

Figure 1. Normalized absorption spectra of CoOEP in chloroform and the CoOEP porphyrins adsorbed on CVD, ARC, CG200x, CG100, SG76, and SG65 SWCNTs after solubilization in 1%DOC/D_2O. For the nanohybrids, the SWCNT reference spectrum is subtracted as described in the text. Note that the longer wavelength Q-band-region is not reliable for the thinnest SWCNTs (SG76, SG65), because these have sharp, intense absorption features overlapping with the Q-bands. The inset zooms in on the Soret band region of the spectrum.

for the SG65 sample might in part be attributed to the lower fraction of M tubes (see below), as M tubes act as significantly stronger electron acceptors than SC tubes for CoOEP.[44] However, by far the dominant factor appears to be the diameter of the tubes (see Table 2). A similar diameter dependence of the absorption spectrum has been observed before for a tetraphenylporphyrin on SWCNTs, and was attributed to a planarization of the phenyl substituents.[49] However, as we observe the same effect here, for a porphyrin without these phenyl groups, a more likely explanation is that the weaker curvature of the walls of thicker tubes results in a better $\pi-\pi$-overlap of the porphyrin with the SWCNTs.

EPR Quantification. The experimental CoOEP probe EPR spectra obtained for each of the SWCNT materials, together with the results from the simultaneous fit are included in Figures 2 and S10−S18 (Supporting Information), and the resulting M:SC ratios are listed in Table 3. The common EPR simulation parameters (including strains) obtained from the simultaneous fit are given in Table 1. An excellent fit is obtained for all samples using this common set of parameters. The M and SC contributions were simulated using axial **g**- and hyperfine tensors in combination with an isotropic Lorentzian line width. To obtain a good fit, it was necessary to include *g*- and hyperfine strains, with a positive correlation of the principal values. The values of these strains are fwhm values of Gaussian distributions of the *g*- and hyperfine values, in such a way that the total line width is a convolution of the isotropic Lorentzian line width and these Gaussian strains.[47] The SC/O_2 contribution was simulated using orthorhombic **g**- and hyperfine tensor frames which are not coinciding, with the Euler angles between the two frames being (0°, β, 0°).[45]

TABLE 2. Red Shift of the Optical Absorption of CoOEP upon Adsorption on Various SWCNT Samples, and Comparison with the Diameter Range *d* of the SWCNTs (as Specified by the Manufacturer)

SWCNT sample	*d* (nm)	red shift (nm)
CVD	2	15
ARC	1.4 ± 0.2	15
CG200x	1.01 ± 0.3	15
CG100	1.0 ± 0.3	14
SG76	0.9 ± 0.2	12
SG65	0.8 ± 0.1	10

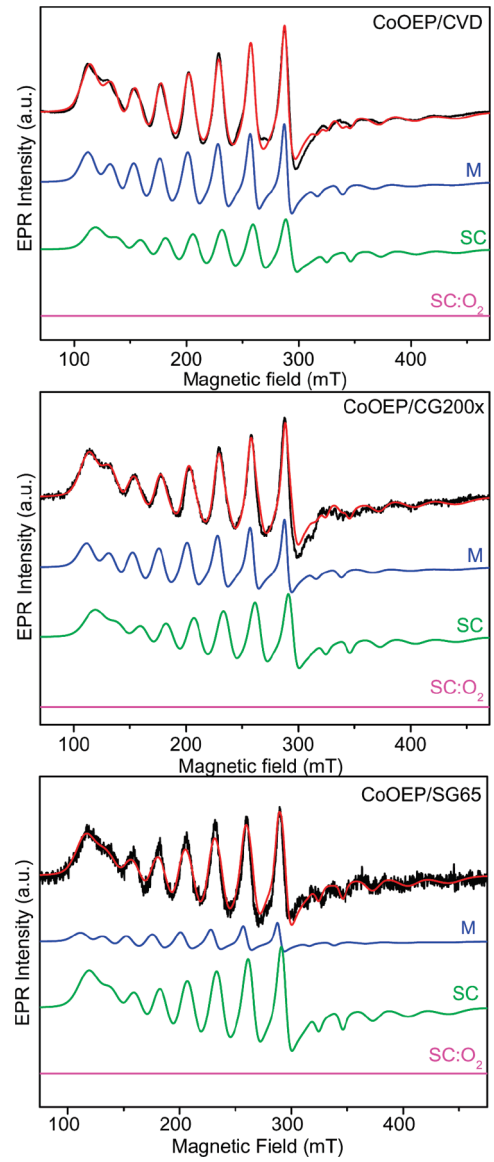

Figure 2. Low temperature (T = 2.5 K, 9.44 GHz) EPR spectra (black) of the different nanohybrid powders with low oxygen content: CoOEP/CVD_1, CoOEP/CG200x_1, and CoOEP/SG65a_1. The simulation (red) which is superimposed on the EPR spectra is composed of a sum of the three contributions: M (blue), SC (green), and SC/O_2 (magenta). The relative coefficients of the different components are given in Table 3. Experimental spectra of CoOEP/CVD SWCNTs were obtained using a more careful exclusion of O_2 and were more accurately fitted than in ref 44.

TABLE 3. M:SC Ratios Determined by Simultaneously Fitting the EPR Spectra

SWCNT materials[a]	Figure	M	SC	SC/O_2	M:SC ratio[b]
CVD_1[c]	2	35%	65%	0%	34.5 ± 2%:65.5 ± 2%
CVD_2	S9	34%	63%	3%	
ARC	S10	29%	65%	6%	29 ± 3%:71 ± 3%
CG200x_1	2	39%	61%	0%	39.5 ± 4%:60.5 ± 4%
CG200x_2	S11	40%	24%	36%	
CG100	S12	42.5%	57.5%	0%	42.5 ± 3%:57.5 ± 3%
SG76_1	S13	34%	66%	0%	32.5 ± 2%:67.5 ± 2%
SG76_2	S14	31%	27%	44%	
SG65a_1	2	15%	85%	0%	16 ± 2%:84 ± 2%
SG65a_2	S15	18%	71%	11%	
SG65a_3	S16	14%	16%	70%	
SG65b	S17	16%	76%	8%	

[a]"_1" stands for preparation in oxygen-poor atmosphere, "_2" and "_3" denotes a larger contribution of oxygenated species. [b]The percentage of SC tubes is obtained by adding the SC and SC/O_2 coefficients. [c]New experimental EPR spectra were obtained for freshly made CoOEP/CVD nanohybrids in oxygen-poor atmosphere and simultaneously analyzed with the new EPR parameters given in Table 1, compared to the results presented in ref 44.

To estimate the error bars on these magnetic parameters, and the effect these have on the final M:SC ratios obtained, fits in which the EPR parameters were optimized for each sample separately were also performed. This yielded no significant further improvement of the fits, and more importantly, no significant change in the obtained M:SC ratios. The largest apparent change of the EPR parameters, though still very small, was observed for SG65a_2, especially for the M component (see error bars in Table 1). Even this change is probably insignificant (within the statistical experimental error), but it might also hint at the effect of reduced $\pi-\pi$-interaction of CoOEP with these very thinnest SWCNTs—which was also found to have a much more pronounced effect on the optical absorption (smaller red-shift; Figure 1). That the tube diameter has much less effect on the EPR parameters can in fact be easily understood because EPR probes the spin-density on the central Co ion, whereas optical absorption originates from the conjugated π-system of the (approximately planar) porphyrin ring. Even for these thinnest tubes the M:SC ratios obtained did not change significantly when optimizing the EPR parameters for this sample specifically, for example, 14%:86% from the individual fit of SG65a_2 compared to 16%:84% on average for these SWCNTs when using the common parameters. Thus, the common set of EPR parameters obtained in this work is valid for any SWCNTs in the studied range, that is, at least down to a diameter of ~0.7 nm (SG65). If the method were extended to even thinner tubes, it would be advisible to check and reoptimize the EPR parameters, especially in view of the optical absorption results. For larger diameter SWCNTs (>2 nm), no changes are expected. Previously,[44] we furthermore found that also the presence of bundles has no effect on the ratio of the two EPR signals, as after solubilization of the CoOEP-coated SWCNTs in water using bile salt surfactant, and removal of the bundles by thorough centrifugation, the same ratio is found, showing that the surface area probed is representative for all tubes in the sample. Of course, care should be taken that the SWCNT samples used are at least reasonably pure with respect to other carbonaceous impurities such as graphitic nanoparticles, double-wall (DWNTs, and multiwall carbon nanotubes (MWNTs), which are likely to adsorb the CoOEP molecules in a similar way and give rise to similar, but different EPR spectra (a limited contamination with graphitic nanoparticles or MWNTs is expected to be less important, as these have a relatively small specific surface area (compared to the SWCNTs)). This is not a problem though, as the distinction between M and SC SWCNTs, and the characterization of the precise M:SC ratio is hardly relevant when the SWCNTs are not pure in the first place: such carbonaceous impurities are far easier to remove from SWCNTs, than it is to separate (or selectively synthesize) M from SC SWCNTs, and most commercially available SWCNT samples (as well as all of the samples used in the present work) do not contain any significant amounts of these. As the SWCNT samples studied in this work originate from different synthesis methods, resulting in very different properties, we can conclude that the EPR parameters of the different components given in Table 1 are not only independent of tube diameter (within the studied range), but are also not influenced by other factors such as defect density, length, bundling, *etc.*, which makes this method unique compared to all other methods already proposed in the literature.[3,20,24,25,27,29,50]

To check that the technique is insensitive to the presence of oxygen, we performed the measurements both in an oxygen-poor atmosphere and in the presence of oxygen. As can be seen from Table 3, the M:SC ratios are nearly independent of the total percentage of SC/O_2 present in the EPR spectrum. Thus it is not critical to exclude oxygen. However, as the SC/O_2 component is much narrower than the M component and therefore much more intense in the derivative EPR spectrum, the simultaneous determination of the M contribution and a dominant SC/O_2 contribution might be expected to result in a somewhat reduced precision. Therefore we recommend performing the experiments in an oxygen-poor atmosphere.

From Table 3, it can be observed that CVD, ARC, and SG76 tubes contain the expected random 1:2 ratio. For the SG65, CG100, and CG200x the M:SC ratios differ strongly from this 1:2 ratio with a larger SC (M) content for the SG65 (CG100, CG200x) tubes, respec-

tively. The observation of a much smaller fraction of M SWCNTs in SG65 (16 ± 2%) is in line with the results from scanning probe microscopy[28] (14 ± 5%), resonant Raman scattering experiments[20] (8%), and the counting by AFM and fluorescence microscopy[29] (8%). As already discussed in the introduction, the slightly different results for the different methods most likely is originating from the difficulty to exclude a bias toward different SWCNT types, diameters, lengths, bundles, defects, *etc*. The important advantage of our method is that it does not have such a bias. The higher M content for CG100 SWCNTs is in agreement with results from the counting by AFM and fluorescence microscopy[29] (48%). Furthermore, films produced with these CG100 SWCNTs and with the CG200x CoMoCAT SWCNTs, which we also found to contain a larger fraction of M SWCNTs (39.5 ± 4%), indeed show a higher conductivity compared to the other CoMoCAT SWCNTs.[51] This novel technique already yields the best accuracy (2−4%) available for the determination of the M:SC ratio of SWCNT samples. Possibly, further improvements of its precision may be achieved by devising other probe molecules with an even higher sensitivity to the electronic type of the SWCNTs.

Having determined the magnetic parameters of all three component spectra with great accuracy, and having established that these are for all practical purposes independent of other factors such as tube length, defect density, and diameter (within the studied range and most likely also for larger diameter SWCNTs), any sufficiently pure SWCNT sample can now be characterized by CoOEP probe EPR. The coefficients a_i of eq 1 are then simply given by a straightforward and robust analytical least-squares regression:

$$\mathbf{A} = (\mathbf{S}'\cdot\mathbf{S})^{-1}\cdot(\mathbf{S}'\cdot\mathbf{S}_{exp}) \qquad (2)$$

where **A** is a column vector containing the three coefficients a_i, $\mathbf{S}_{exp}$ is the column vector containing the experimental spectrum, and **S** is the three-column matrix containing the three component spectra S_i, as simulated by EasySpin using the parameters from Table 1. The M:SC mass ratio is then given by a_1:(a_2 + a_3). Note that it is also possible to incorporate the EPR background subtraction in this same linear regression step, by including (a smooth polynomial fit to) the SWCNT background spectrum as a fourth basis function S_4 in **S**.

CONCLUSIONS

An accurate and easy spectroscopic technique to quantify the ratio of M to SC SWCNTs from a single experiment on a bulk SWCNT sample is presented. After noncovalent functionalization of the SWCNTs with Cobalt(II)octaethylporphyrins (CoOEP) the EPR spectrum of CoOEP/SWCNT nanohybrid powders is measured (preferably, but not necessarily, in oxygen-poor atmosphere). The CoOEP molecules probe the different electronic interactions of the cobalt ion (spin density distribution) with M and SC tubes, which is reflected in the observation of two distinct EPR spectra. These signals are easily distinguished and accurately characterized in this work, allowing the intensities of both signals to be determined from a robust, analytical least-squares fit of the measured EPR spectra for arbitrary SWCNT samples. As the EPR intensity can be directly related to the number of spins, that is, the number of CoOEP molecules, and as the adsorption of CoOEP (π−π-stacking) is itself found to be unbiased toward metallic or semiconducting tubes, the obtained intensities of the least-squares fit can be directly related to the mass percentage of metallic and semiconducting tubes in the bulk SW SWCNT samples. We were able to accurately determine the M:SC ratio for six different types of SWCNT materials originating from various sources. For three different samples (CVD, ARC, and SG76 CoMoCAT) a M:SC ratio very close to the random 1:2 ratio was observed: 34.5%:65.5% for CVD, 29%:71% for ARC, and 32.5%:67.5% for SG76 SWCNTs. For SG65 CoMoCAT SWCNTs a M:SC ratio of 16%:84% was determined, in line with results already obtained in the literature. For CG100 and CG200x CoMoCAT SWCNTs, a larger metallic fraction was observed, yielding a M:SC ratio of 42.5%:57.5% and 39.5%:60.5%, respectively. Considering that these different SWCNT materials have different diameters, diameter distributions, and also different lengths/defect densities, it can be concluded that the proposed method is unaffected by a wide range of other properties and can therefore be used for the reliable quantification of the M:SC ratio of SWCNT samples.

METHODS

SWCNT Samples. A series of SWCNT materials, having different average tube diameters and diameter distributions and synthesized by different methods were analyzed in this study. These include SWCNTs produced by the catalytic carbon vapor deposition process obtained from Nanocyl (batch no. NRJ21; SWCNT content, 60%) with an average diameter of 2 nm (CVD) and which were also studied in our previous work;[44] arc-discharge SWCNTs obtained from Nanoledge (raw, batch no. P00508D; SWCNT content 30%) with a mean diameter of 1.4 ± 0.2 nm, which were further purified using air oxidation, acid treatment, and high vacuum annealing as described in ref 38 (ARC). We also studied four different SWCNT materials produced by the cobalt/molybdenum-catalyst-based synthesis method (CoMoCAT) developed at the University of Oklahoma[2] and obtained from SouthWest NanoTechnologies (SWeNT): (1) CG200x SWCNTs having a diameter range of 1.01 ± 0.3 nm (>90% carbon content, lot no. 400), (2) CG100 SWCNTs having a diameter range of 1.0 ± 0.3 nm (>90% carbon content, lot no. 000-0012) (3) SG65 SWCNTs (>90% carbon content) having a tube diameter of 0.8 ± 0.1 nm and a composition rich in (6,5) and semiconducting tubes, two different batches of which were studied (SG65a, lot no. 000-0031 (SWeNT); SG65b, lot no. 000-000-010) and (4) SG76 SWCNTs having a tube diameter of 0.9 ± 0.2 nm and rich in

(7,6) tubes (>90% carbon content, lot no. 000-0014). We also applied this method to study purified HipCO SWCNTs obtained from Carbon Nanotechnologies, Inc. (2 wt % of Fe residues, batch no. SP0235).

Sample Preparation. The porphyrin nanohybrids were prepared for EPR and optical spectroscopy using a modified procedure from ref 44, using 2,3,7,8,12,13,17,18-octaetyl-21*H*,23*H*-porphyrin cobalt(II) (CoOEP) obtained from Aldrich. The SWCNTs (10 mg) were added to a saturated solution (3 mL) of CoOEP in chloroform (99+%, stabilized with 0.6% ethanol, VWR Prolabo BDH). Ultrasound (bath sonicator: BRANSONIC, 1510E-MTH, 70 W, 42 kHz) was applied for 1 h each of 3 subsequent days, in order to obtain a fine dispersion of the SWCNTs, thereby increasing the contact area for the porphyrin molecules to adsorb. In between the ultrasonic treatments the samples were magnetically stirred in the dark. Afterward, the solution was filtrated (Zefluor, supported PTFE membrane, 0.5 μm pore size) and rinsed several times with chloroform until the filtrate was colorless. The dried porphyrin/SWCNT pellet was peeled off the filter membrane and gently ground to obtain a powder: CoOEP/CVD, CoOEP/ARC, CoOEP/CG200x, CoOEP/CG100, CoOEP/SG65a, and CoOEP/SG65b, CoOEP/SG76 and CoOEP/HipCO. These powders were then measured in EPR. Furthermore, in contrast to our previous work,[44] part of the powders were put in an oxygen-poor nitrogen atmosphere for 1 day and sealed before the EPR experiments, in order to avoid large contributions in the EPR spectra from oxygenated species.

EPR Spectroscopy. The continuous-wave (CW) EPR (X-band, 9.44 GHz) spectra were recorded at 2.5 K in the rectangular cavity of a Bruker ESP300E spectrometer equipped with an Oxford liquid helium flow cryostat. Measurements can also be performed with similar signal-to-noise ratio at slightly higher temperatures (5−10 K) depending on the SWCNT background spectrum (see Supporting Information). A microwave power of 12.6 mW (12 dB), modulation amplitude of 0.2 mT, and modulation frequency of 100 kHz were used. For a single EPR experiment, 1 mg of the porphyrin-functionalized SWCNTs was introduced in the EPR tube, which is sufficient to obtain a good signal-to-noise ratio. For each of the samples an EPR spectrum of the SWCNT powders without the porphyrin functionalization was measured in EPR and used as a background, which was subtracted from the obtained spectra, after multiplication by a weight factor, in order to obtain a flat baseline.

Absorption Spectroscopy. Absorption spectra were recorded with a Varian Cary 5E UV−vis−IR spectrometer, using quartz cells with path lengths of 0.1, 1, or 10 mm. For the solubilization, a part (5 mg) of each of the SWCNT powders was added to a 1% w/v sodium deoxycholate (DOC, 99%, Acros Organics) solution (1.5 mL) in D_2O (99.9 atom % D, Aldrich). Afterward the solutions were centrifuged for 30 min at 16215*g* (Sigma 2-16KCH centrifuge with swing-out rotor) and the supernatant was collected.[18]

Acknowledgment. The authors wish to thank J. B. Nagy and A. Fonseca (Nanocyl) for providing the CVD SWCNTs. Financial support from both the Fund for Scientific Research Flanders, Belgium, (FWO-Vlaanderen, project G.0129.07) and the Hercules Foundation, Flanders, (contract AUHA013) is gratefully acknowledged. The research was partly performed in the framework of the SBO-project 060843 "PolySpec" funded by the Institute for the Promotion of Innovation by Science and Technology in Flanders (IWT).

Supporting Information Available: EPR spectra of the raw SWCNT samples, absorption spectra of the solubilized nanohybrids, and additional EPR spectra and simulations of the different nanohybrid powders. This material is available free of charge *via* the Internet at http://pubs.acs.org.

REFERENCES AND NOTES

1. Reich, S.; Thompson, C.; Maultzsch, J. *Carbon Nanotubes: Basic Concepts and Physical Properties*; Wiley-VCH: Berlin, 2004.
2. Kitiyanan, B.; Alvarez, W. E.; Harwell, J. H.; Resasco, D. E. Controlled Production of Single-Wall Carbon Nanotubes by Catalytic Decomposition of CO on Bimetallic Co−Mo Catalysts. *Chem. Phys. Lett.* **2000**, *317*, 497–503.
3. Li, Y.; Mann, D.; Rolandi, M.; Kim, W.; Ural, A.; Hung, S.; Javey, A.; Cao, J.; Wang, D.; Yenilmez, E.; *et al.* Preferential Growth of Semiconducting Single-Walled Carbon Nanotubes by a Plasma Enhanced CVD Method. *Nano Lett.* **2004**, *4*, 317–321.
4. Harutyunyan, A. R.; Chen, G. G.; Paronyan, T. M.; Pigos, E. M.; Kuznetsov, O. A.; Hewaparakrama, K.; Kim, S. M.; Zakharov, D.; Stach, E. A.; Sumanasekera, G. U. Preferential Growth of Single-Walled Carbon Nanotubes with Metallic Conductivity. *Science* **2009**, *326*, 116–120.
5. Ding, L.; Tselev, A.; Wang, J. Y.; Yuan, D. N.; Chu, H. B.; McNicholas, T. P.; Li, Y.; Liu, J. Selective Growth of Well-Aligned Semiconducting Single-Walled Carbon Nanotubes. *Nano Lett.* **2009**, *9*, 800–805.
6. Bachilo, S. M.; Balzano, L.; Herrera, J. E.; Pompeo, F.; Resasco, D. E.; Weisman, R. B. Narrow (*n*,*m*)-Distribution of Single-Walled Carbon Nanotubes Grown Using a Solid Supported Catalyst. *J. Am. Chem. Soc.* **2003**, *125*, 11186–11187.
7. Arnold, M. S.; Green, A. A.; Hulvat, J. F.; Stupp, S. I.; Hersam, M. C. Sorting Carbon Nanotubes by Electronic Structure Using Density Differentiation. *Nat. Nanotechnol.* **2006**, *1*, 60–65.
8. Duesberg, G. S.; Burghard, M.; Muster, J.; Philipp, G.; Roth, S. Separation of Carbon Nanotubes by Size Exclusion Chromatography. *Chem. Commun.* **1998**, *3*, 435–436.
9. Hennrich, F.; Lebedkin, S.; Kappes, M. M. Improving Separation Techniques for Single-Walled Carbon Nanotubes: Towards Monodisperse Samples. *Phys. Stat. Sol. B* **2008**, *245*, 1951–1953.
10. Hersam, M. C. Progress Towards Monodisperse Single-Walled Carbon Nanotubes. *Nat. Nanotechnol.* **2008**, *3*, 387–394.
11. Krupke, R.; Hennrich, F. Separation Techniques for Carbon Nanotubes. *Adv. Eng. Mater.* **2005**, *7*, 111–116.
12. Miyata, Y.; Maniwa, Y.; Kataura, H. Selective Oxidation of Semiconducting Single-Wall Carbon Nanotubes by Hydrogen Peroxide. *J. Phys. Chem. B* **2006**, *110*, 25–29.
13. Song, J. W.; Seo, H. W.; Park, J. K.; Kim, J. E.; Cho, D. G.; Han, C. S. Selective Removal of Metallic SWNTs Using Microwave Radiation. *Curr. Appl. Phys.* **2008**, *8*, 725–728.
14. Tanaka, T.; Jin, H.; Miyata, Y.; Fujii, S.; Suga, H.; Naitoh, Y.; Minari, T.; Miyadera, T.; Tsukagoshi, K.; Kataura, H. Simple and Scalable Gel-Based Separation of Metallic and Semiconducting Carbon Nanotubes. *Nano Lett.* **2009**, *9*, 1497–1500.
15. Zheng, M.; Jagota, A.; Semke, E. D.; Diner, B. A.; Mclean, R. S.; Lustig, S. R.; Richardson, R. E.; Tassi, N. G. DNA-Assisted Dispersion and Separation of Carbon Nanotubes. *Nat. Mater.* **2003**, *2*, 338–342.
16. Roberts, M. E.; LeMieux, M. C.; Sokolov, A. N.; Bao, Z. N. Self-Sorted Nanotube Networks on Polymer Dielectrics for Low-Voltage Thin-Film Transistors. *Nano Lett.* **2009**, *9*, 2526–2531.
17. Haddon, R. C.; Sippel, J.; Rinzler, A. G.; Papadimitrakopoulos, F. Purification and Separation of Carbon Nanotubes. *MRS Bull.* **2004**, *29*, 252–259.
18. Wenseleers, W.; Vlasov, I. I.; Goovaerts, E.; Obraztsova, E. D.; Lobach, A. S.; Bouwen, A. Efficient Isolation and Solubilization of Pristine Single-Walled Nanotubes in Bile Salt Micelles. *Adv. Funct. Mater.* **2004**, *14*, 1105–1112.
19. Green, A. A.; Duch, M. C.; Hersam, M. C. Isolation of Single-Walled Carbon Nanotube Enantiomers by Density Differentiation. *Nano Res.* **2009**, *2*, 69–77.
20. Jorio, A.; Santos, A. P.; Ribeiro, H. B.; Fantini, C.; Souza, M.; Vieira, J. P. M.; Furtado, C. A.; Jiang, J.; Saito, R.; Balzano, L.; *et al.* Quantifying Carbon Nanotube Species with Resonance Raman Scattering. *Phys. Rev. B* **2005**, *72*, 075207.
21. Popov, V. N.; Henrard, L.; Lambin, P. Resonant Raman Intensity of the Radial Breathing Mode of Single-Walled

Carbon Nanotubes within a Nonorthogonal Tight-Binding Model. *Nano Lett.* **2004**, *4*, 1795–1799.
22. Popov, V. N.; Henrard, L.; Lambin, P. Resonant Raman Intensity of the Radial-Breathing Mode of Single-Walled Carbon Nanotubes. *AIP Conf. Proc.* **2005**, *786*, 465–468.
23. Popov, V. N.; Henrard, L.; Lambin, P. Electron-Phonon and Electron-Photon Interactions and Resonant Raman Scattering from the Radial-Breathing Mode of Single-Walled Carbon Nanotubes. *Phys. Rev. B* **2005**, *72*, 035436.
24. Miyata, Y.; Yanagi, K.; Maniwa, Y.; Kataura, H. Optical Evaluation of the Metal-To-Semiconductor Ratio of Single-Wall Carbon Nanotubes. *J. Phys. Chem. C* **2008**, *112*, 13187–13191.
25. Nair, N.; Usrey, M. L.; Kim, W. J.; Braatz, R. D.; Strano, M. S. Estimation of the (*n*,*m*) Concentration Distribution of Single-Walled Carbon Nanotubes from Photoabsorption Spectra. *Anal. Chem.* **2006**, *78*, 7689–7696.
26. Fagan, J. A.; Simpson, J. R.; Bauer, B. J.; De Paoli Lacerda, S. H.; Becker, M. L.; Chun, J.; Migler, K. B.; Hight Walker, A. R.; Hobbie, E. K. Length-Dependent Optical Effects in Single-Wall Carbon Nanotubes. *J. Am. Chem. Soc.* **2007**, *129*, 10607–10612.
27. Kim, W. J.; Lee, C. Y.; O'brien, K. P.; Plombon, J. J.; Blackwell, J. M.; Strano, M. S. Connecting Single Molecule Electrical Measurements to Ensemble Spectroscopic Properties for Quantification of Single-Walled Carbon Nanotube Separation. *J. Am. Chem. Soc.* **2009**, *131*, 3128–3129.
28. Lu, W.; Xiong, Y.; Hassanien, A.; Zhao, W.; Zheng, M.; Chen, L. W. A Scanning Probe Microscopy Based Assay for Single-Walled Carbon Nanotube Metallicity. *Nano Lett.* **2009**, *9*, 1668–1672.
29. Naumov, A. V.; Kuznetsov, O. A.; Harutyunyan, A. R.; Green, A. A.; Hersam, M. C.; Resasco, D. E.; Nikolaev, P. N.; Weisman, R. B. Quantifying the Semiconducting Fraction in Single-Walled Carbon Nanotube Samples through Comparative Atomic Force and Photoluminescence Microscopies. *Nano Lett.* **2009**, *9*, 3203–3208.
30. Chauvet, O.; Forro, L.; Bacsa, W.; Ugarte, D.; Doudin, B.; Deheer, W. A. Magnetic Anisotropies of Aligned Carbon Nanotubes. *Phys. Rev. B* **1995**, *52*, R6963–R6966.
31. Coleman, J. N.; O'Brien, D. F.; Dalton, A. B.; McCarthy, B.; Lahr, B.; Barklie, R. C.; Blau, W. J. Electron Paramagnetic Resonance as a Quantitative Tool for the Study of Multiwalled Carbon Nanotubes. *J. Chem. Phys.* **2000**, *113*, 9788–9793.
32. Corzilius, B.; Dinse, K. P.; Hata, K. Single-Wall Carbon Nanotubes and Peapods Investigated by EPR. *Phys. Chem. Chem. Phys.* **2007**, *9*, 6063–6072.
33. Salvetat, J. P.; Feher, T.; L'Huillier, C.; Beuneu, F.; Forro, L. Anomalous Electron Spin Resonance Behavior of Single-Walled Carbon Nanotubes. *Phys. Rev. B* **2005**, *72*, 075440.
34. Petit, P.; Jouguelet, E.; Fischer, J. E.; Rinzler, A. G.; Smalley, R. E. Electron Spin Resonance and Microwave Resistivity of Single-Wall Carbon Nanotubes. *Phys. Rev. B* **1997**, *56*, 9275–9278.
35. Corzilius, B.; Dinse, K. P.; Hata, K.; Haluska, M.; Skakalova, V.; Roth, S. SWNT Probed by Multifrequency EPR and Nonresonant Microwave Absorption. *Phys. Stat. Sol. B* **2008**, *245*, 2251–2254.
36. Corzilius, B.; Gembus, A.; Weiden, N.; Dinse, K. P. Preparation and EPR Characterization of N@C-60 and N@C-70 Based Peapods. *AIP Conf. Proc.* **2005**, *786*, 317–320.
37. Simon, F. Studying Single-Wall Carbon Nanotubes Through Encapsulation: From Optical Methods till Magnetic Resonance. *J. Nanosc. Nanotechnol.* **2007**, *7*, 1197–1220.
38. Cambré, S.; Wenseleers, W.; Goovaerts, E. Endohedral Copper(II)acetylacetonate/Single-Walled Carbon Nanotube Hybrids Characterized by Electron Paramagnetic Resonance. *J. Phys. Chem. C* **2009**, *113*, 13505–13514.
39. D'Souza, F.; Ito, O. Supramolecular Donor−Acceptor Hybrids of Porphyrins/Phthalocyanines with Fullerenes/Carbon Nanotubes: Electron Transfer, Sensing, Switching, and Catalytic Applications. *Chem. Commun.* **2009**, *33*, 4913–4928.
40. Langa, F.; Gomez-Escalonilla, M. J.; de la Cruz, P. Carbon Nanotubes and Porphyrins: An Exciting Combination for Optoelectronic Devices. *J. Porphyrin Phthalocyanines* **2007**, *11*, 348–358.
41. Guldi, D. M. Nanometer Scale Carbon Structures for Charge-Transfer Systems and Photovoltaic Applications. *Phys. Chem. Chem. Phys.* **2007**, *9*, 1400–1420.
42. Basiuk, V. A.; Contreras-Torres, F. F.; Bassiouk, M.; Basiuk, E. V. Interactions of Porphyrins with Low-Dimensional Carbon Materials. *J. Comput. Theor. Nanosci.* **2009**, *6*, 1383–1411.
43. Lin, W. C., Electron Spin Resonance and Electronic Structure of Metalloporphyrins. In *The Porphyrins*; Dolphin, D., Ed.; Academic Press: New York, 1978−1979; Vol. 4, pp 335−377.
44. Cambré, S.; Wenseleers, W.; Culin, J.; Van Doorslaer, S.; Fonseca, A.; B. Nagy, J.; Goovaerts, E. Characterisation of Nanohybrids of Porphyrins with Metallic and Semiconducting Carbon Nanotubes by EPR and Optical Spectroscopy. *ChemPhysChem* **2008**, *9*, 1930–1941.
45. Walker, F. A. An Electron Spin Resonance Study of Coordination to Fifth Position and Sixth Position of α,β,γ,δ-Tetra(*P*-methoxyphenyl)porphinatocobalt(II). *J. Am. Chem. Soc.* **1970**, *92*, 4235–4244.
46. Walker, F. A. ESR Studies of Co(II) Tetraphenylporphyrins and Their Oxygen Adducts−Complex Formation with Aromatic Molecules and Sterically Hindered Lewis Bases. *J. Magn. Reson.* **1974**, *15*, 201–218.
47. Stoll, S.; Schweiger, A. EasySpin, A Comprehensive Software Package for Spectral Simulation and Analysis in EPR. *J. Magn. Reson.* **2006**, *178*, 42–55.
48. Svistunenko, D. A.; Sharpe, M. A.; Nicholls, P.; Wilson, M. T.; Cooper, C. E. A New Method for Quantitation of Spin Concentration by EPR Spectroscopy: Application To Methemoglobin and Metmyoglobin. *J. Magn. Reson.* **2000**, *142*, 266–275.
49. Magadur, G.; Lauret, J. S.; Alain-Rizzo, V.; Voisin, C.; Roussignol, P.; Deleporte, E.; Delaire, J. A. Excitation Transfer in Functionalized Carbon Nanotubes. *ChemPhysChem* **2008**, *9*, 1250–1253.
50. Liu, X.; Pichler, T.; Knupfer, M.; Golden, M. S.; Fink, J.; Kataura, H.; Achiba, Y. Detailed Analysis of the Mean Diameter and Diameter Distribution of Single-Wall Carbon Nanotubes from Their Optical Response. *Phys. Rev. B* **2002**, *66*, 045411.
51. Tan, Y.; Prada Silvy, R., SouthWest Nanotechnologies (Private Communication, 2010).